Journal of Radioanalytical and Nuclear Chemistry (2023) 332:3977–3990
https://doi.org/10.1007/s10967-023-09091-0

High-efficiency removal of U(VI) from low-concentration uranium-bearing wastewater using $ZnCl_2$-modified activated carbon loading nZVI

Qi Fang[1] · Jing Wang[1] · Qian Liu[1] · Yanling Tan[1] · Zhenyu Chen[1] · Junwen Lv[1] · De Zhang[1] · Guojian Peng[2]

Received: 4 April 2023 / Accepted: 27 July 2023 / Published online: 30 August 2023

Abstract

$ZnCl_2$-modified activated carbon supported nanoscale zero-valent iron material (nZVI/BC600) was synthesized by green carbothermal reduction and liquid phase reduction to explore the removal efficiency of U(VI) under different conditions. The results showed that under the optimal conditions (C_0 = 10 mg/L, C/Fe = 5:1, pH = 5.5, t = 30 min), the removal rate of U(VI) by nZVI/BC600 was 99.68%, which was 9.18% higher than that of $ZnCl_2$-modified activated carbon and conformed to the pseudo-second-order kinetic model. SEM and XPS analysis showed that nZVI was uniformly distributed on activated carbon, and U(VI) was reduced to U(IV) or U(V). The removal mechanism of U(VI) by nZVI/BC600 is chemical adsorption, redox and co-precipitation.

Keywords Activated carbon · U(VI) removal · Nano-zero-valent iron (nZVI) · $ZnCl_2$

Introduction

Uranium is an important raw material of natural resources for nuclear energy. With the continuous expansion of nuclear energy application and development, a large amount of radioactive uranium-containing wastewater is generated during uranium mining, nuclear facility use, decommissioning, nuclear leakage and other processes [1]. Uranium has radiation and chemical toxicity, but it is notoriously difficult to be absorbed by plants or degraded by microorganisms in the ecosystem, so it causes great harm to plants and animals [2]. For the sake of ecological environment and human health, Chinese relevant regulations stipulate that the maximum permissible concentration of natural uranium is about 40 μg/L, while the average concentration of natural uranium in inland rivers is 0.5 μg/L [3]. In general, uranium concentration in drinking water is less than 1 μg/L. According to the survey, the total uranium concentration in drinking water sources from 2010 to 2018 was 0.09~4.50 μg/L [4]. U(VI) mainly exists in the form of uranyl ions (UO_2^{2+}) in solution, and often forms anion complexes with OH^-, CO_3^{2-}, SO_4^{2-}, PO_4^{3-}, etc. [5]. Uranyl ion has enormous ionic radius and is characterized by freely solubility, high toxicity and easy to migrate. However, tetravalent U(IV) is insoluble and can be easily precipitated as uranium dioxide (UO_2) or can be oxidized to U(VI). Therefore, it is widely recognized to be one of the most promising approaches to reduce the soluble hexavalent U(VI) into insoluble tetravalent U(IV) containing minerals [6–8].

In the treatment of U(VI)-bearing wastewater, the economical and efficient adsorption methods are widely used. Nevertheless, the adsorbent can only enrich U(VI) and gather, but cannot reduce its biological toxicity, and it would even desorb and re-enter the water to produce pollution. Hence, zero-valent iron and nano-zero-valent iron (nZVI) treatment of heavy metal pollution wastewater came into existence [9–13]. nZVI has stronger reduction characteristics, larger specific surface area, stronger adsorb ability and higher removal efficiency than ordinary zero-valent iron. Nonetheless, like other nanomaterials [14, 15], they are characterized by small particle size, great specific surface area, high reduction activity and huge magnetic force. They are easy to accumulate and be oxidized. While causing

✉ Qi Fang
frances2009@foxmail.com

[1] School of Resource Environment and Safety Engineering, University of South China, Hengyang 421001, People's Republic of China

[2] School of Computer Science, University of South China, Hengyang 421001, People's Republic of China

secondary pollution, their reactivity in water and removal efficiency of pollutants are greatly reduced, which poses a challenge to the practical application of nZVI. To solve these problems, researchers have been looking at a variety of stable materials [16–33], nZVI is dispersed on activated carbon [34–39], zeolite [40, 41], clay minerals [42] and biomolecular materials [43] to reduce or even prevent agglomeration and improve its dispersion and stability [44, 45]. While retaining the inherent characteristics of nZVI, it overcomes shortcomings and improves the reaction performance [46].

Among all kinds of stable materials, the environmentally friendly and inexpensive activated carbon is the most common application. Activated carbon is a form of highly aromatic and insoluble solid substance [47], which is prepared by plant, crop waste, activated sludge, etc., under the condition of oxygen restriction [48–51]. In the past few decades, biochar supported nZVI has been shown to be more effective than bare nZVI in the treatment of heavy metal contamination [52] and organic compounds [53]. A novel material that nZVI loaded on biochar with stable starch stabilization (nZVI/BC) was synthesized and used for the removal of vanadium V(V) [54] and hexavalent chromium Cr(VI) [55] in simulated wastewater. Li X et al. [8] studied the montmorillonite supported nZVI adsorption materials, which was synthesized by sodium borohydride and ferric chloride. The results showed that montmorillonite loaded nZVI reacted quickly (about 3 min after the start of the reaction), the removal rate of uranium solution with 100 μg/L was up to 97.8%, which was much higher than that of montmorillonite (48.0%) and nZVI (79.5%) under the optimal conditions. Jing et al. [10] showed that illite-loaded nZVI can remove 99.9% uranium in groundwater within 2 h, the uranium concentration remained at about 27 mg/L after 7 days of reaction time, and there was no sign of uranium release in groundwater. The effect of pH on the removal efficiency and the stability of uranium in the material were also studied, resulting that the supported material has better properties than the single nZVI. Yan et al. [56] used nZVI and biochar loaded nZVI as additives to activate persulphate to oxidize trichlene in groundwater, and the results showed that the activation performance of nZVI supported by biochar was significantly higher than that of nZVI.

In the present work, activated carbon was prepared by peanut shells and $ZnCl_2$ was used for modification since previous studies proved that $ZnCl_2$ could improve activated carbon's adsorption performance through catalytic dehydration, bloating and pore-making effects [57–60]. The composite material marked as nZVI/BC600 was synthesized by dispersing nZVI particles onto the surface and pores of the prepared activated carbon. After that, batch experiments were carried out to investigate the effects of reaction time, initial pH, dosage, and coexisting ions on the removal rate of U(VI) from aqueous solution. The kinetic model was used to analyze the kinetic rule of the adsorption U(VI) of the material. Finally, the microscopic morphology, chemical composition, Chemical valence state and various features of functional groups of the nZVI/BC600 composite material before and after removing U(VI) were analyzed, to elucidate the possible adsorption mechanisms for the removal of U(VI).

Materials and methods

Materials

All chemicals used in the present study were of analytical grade. Postassium borohydride (KBH_4), zinc chloride ($ZnCl_2$) and ferrous sulfate heptahydrate ($FeSO_4{\cdot}7H_2O$) were used for making the composite material. Manganese chloride ($MnCl_2$), magnesium chloride ($MgCl_2$), calcium chloride ($CaCl_2$), sodium sulfate (Na_2SO_4) and sodium bicarbonate ($NaHCO_3$) were applied to study the effect of different ions on the reaction. Dissolved U_3O_8 (of > 99% purity) in concentrated hydrochloric acid (HCl), hydrogen peroxide (H_2O_2) and nitric acid solutions (HNO_3) for preparing the U(VI) stock solution. The deionized water was deoxygenated with high purity nitrogen (99.999%) for 30 min prior to use for the preparation of all solutions.

Experiment methods

Preparation of $ZnCl_2$-modified activated carbon loading nano-zero-valent iron

In the present work, activated carbon was prepared by peanut shells. Zinc chloride was used for its modification, since it could improve adsorption performance by activated carbon through catalytic dehydration, bloating and pore-making effects, that was based on the previous literature methods [58, 61]. The peanut shells were washed thoroughly with tap water followed by deionized water several times to remove impurities and oven-dried, subsequently, crushed and ground into powders to pass through 20-mesh sieves. Then added an appropriate amount of $ZnCl_2$ solution with a mass concentration of 30% to the particles, stirred in a beaker to make it fully mixed, soaked for 14 h and then dried. The sample was placed in a tube furnace, heated to 600 °C at a rate of 5 °C/min, and maintained at high temperature for 30 min under nitrogen conditions. Then the tube furnace was closed and removed after cooling. Afterward, the prepared activated carbon was treated with 1% HCl solution for an hour and the effluent was washed with deionized water while stirring until the pH reached neutral. Finally, the activated carbon was oven-dried, sealed in a brown bottle and labeled as BC600.

$ZnCl_2$-modified activated carbon loading nano-zero-valent iron was prepared by liquid phase reduction method

as reported [62, 63]: 5.0 g $FeSO_4{\cdot}7H_2O$ was dissolved in deionized water under the condition of oscillation and added with a certain volume of anhydrous ethanol as the dispersing agent (alcohol:water ratio = 4:1). Whereafter BC600 was added (C:Fe mass ratio = 5:1) into the mixture followed by dropwise addition of 50 mL freshly prepared $NaBH_4$ solution (20 g/L), with magnetic stirring (200 r/min) under the nitrogen-protected environment. After reaction, the resultant suspension was aged for one hour under nitrogen purging, and the composite was separated by filtration and washed repeatedly with anhydrous ethanol and deionized water. Finally, the resultant materials were oven-dried at 80 °C for 12 h, ground into powders and stored in a desiccator, called as nZVI/BC600 composite. Figure 1 showed a schematic diagram of the experimental procedure that used to synthesize nZVI/BC600, and the reaction chemical equation was described as following.

$$2Fe^{2+} + BH_4^- + 2H_2O = 2Fe + BO_2^- + 2H_2O + 4H^+ \quad (1)$$

Batch experiments

All batch experiments were carried out in a temperature-controlled oscillator at 25 °C and 150 r/min conditions using 100 mL conical flasks. At first, before each set of batch experiments, the pH of 50 mL U(VI) solution (10 mg/L) was adjusted to 5.5 with HCl solution and/or NaOH solution. After which, the U(VI) removal efficiency was investigated at different time intervals (2, 5, 10, 15, 20, 25, 30, 60 and 120 min) in different concentrations (0.05, 0.2, 0.4, 0.6, 0.8 and 1.0 g/L), containing coexisting ions (Mg^{2+}, Mn^{2+}, Ca^{2+}, SO_4^{2-}, HCO_3^- and PO_4^{3-}) and initial pH (2, 3, 4.5, 6, 7, 8.5 and 10). After reaction, solution samples were taken and filtered for the analysis of uranium content and pH value, and the calculation of U(VI) concentration, removal rate and adsorption amount. In order to reduce the experimental error, all experiments were carried out in triplicate and the average data was recorded. The removal capacity and efficiency of U(VI) adsorbed at each time were calculated using the Eqs. (2) and (3), respectively.

$$P = (C_0 - C_e)/C_0 \times 100\% \quad (2)$$

$$q_e = V(C_0 - C_e)/m \quad (3)$$

where P is the removal capacity of U(VI) (%), C_0 is the initial concentration of U(VI) (mg/L); C_e is the concentration of U(VI) in the solution after reaction (mg/L); q_e is the amount of U(VI) adsorbed on the adsorbent per unit mass (mg/g); V is the volume of the solution (L); m is the mass of the adsorbent (g).

Characterization

The working current and voltage of the X-ray diffractometer (XRD, Bruker D8, Germany Bruker Technology Co., Ltd.) were 40 mA and 40 kV, respectively, and the 2θ range was 10°~80°. The magnetic properties were characterized by vibrating sample magnetometer (VSM, ADE-EV7) in the magnetic field range of − 30,000e~30,000e. The surface morphology and structure of the samples before and after the reaction were observed by high resolution field emission scanning electron microscopy (SEM, SUPRATM5, Jieou Luke Trading Co., Ltd.). The surface element composition was detected by energy dispersive X-ray spectroscopy (EDS) and the surface element distribution map was obtained. The specific surface area of the material was measured by V-Sorb 2800P automatic specific surface area and pore size distribution analyzer. The chemical structure was identified by Fourier transform infrared spectroscopy (FT-IR, Nicolet 460, Semmerfeld Technology Co., Ltd.), and the functional groups were scanned in the range of 400~4000 cm^{-1}. The chemical valence of the elements on the surface of the sample was determined by X-ray photoelectron spectroscopy (XPS, Escalab 250Xi, Thermo Fisher Scientific Co., Ltd.). The C 1 s peak at 284.8 eV was used to correct the binding energy.

Fig. 1 The process diagram of synthesis nZVI/BC600 in this experiment

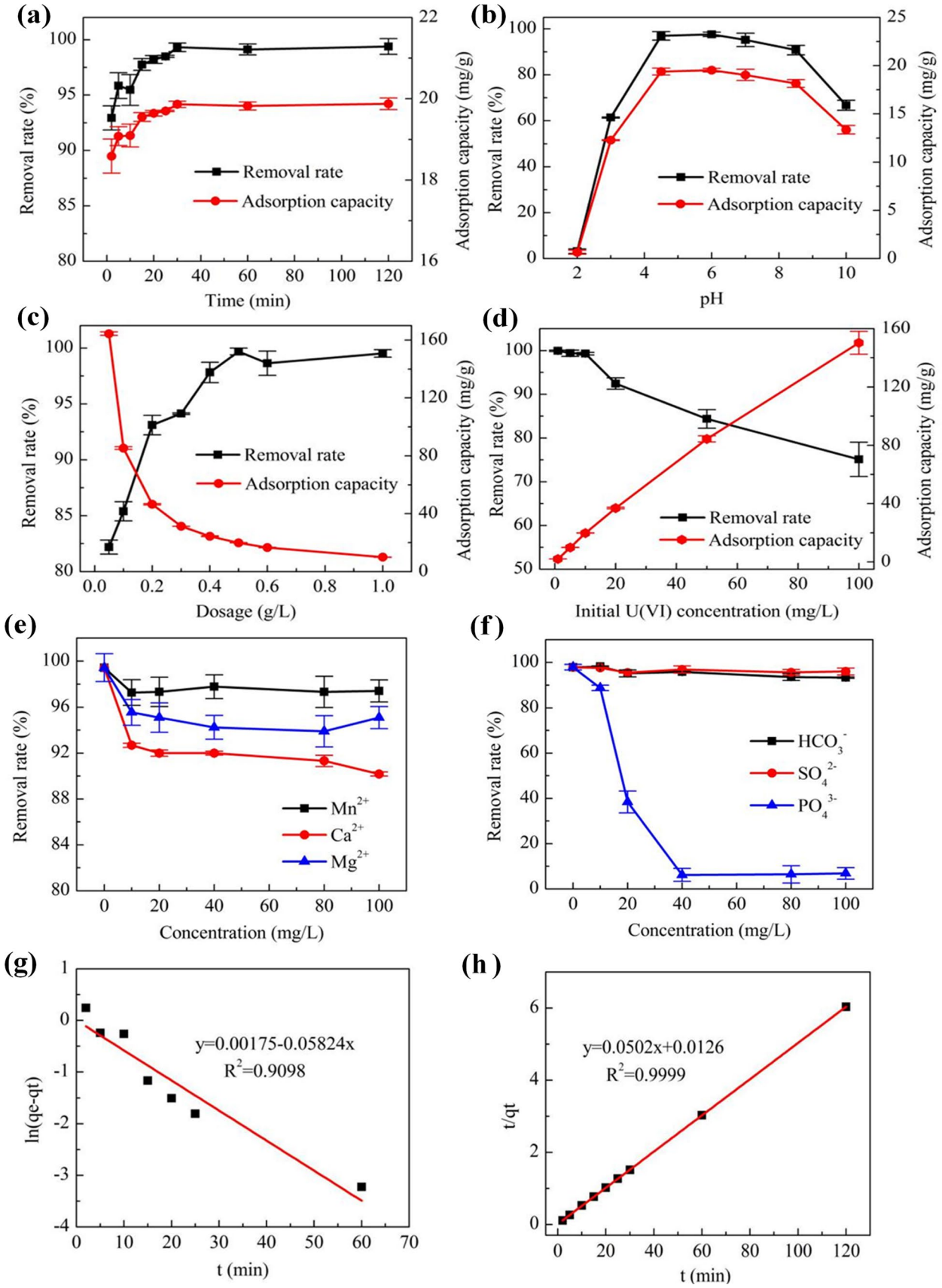
(a)
Removal rate (%)
Adsorption capacity (mg/g)
Time (min)
Removal rate
Adsorption capacity
(b)
Removal rate (%)
Adsorption capacity (mg/g)
pH
Removal rate
Adsorption capacity
(c)
Removal rate (%)
Adsorption capacity (mg/g)
Dosage (g/L)
Removal rate
Adsorption capacity
(d)
Removal rate (%)
Adsorption capacity (mg/g)
Initial U(VI) concentration (mg/L)
Removal rate
Adsorption capacity
(e)
Removal rate (%)
Concentration (mg/L)
Mn2+
Ca2+
Mg2+
(f)
Removal rate (%)
Concentration (mg/L)
HCO3-
SO4 2-
PO4 3-
(g)
ln(qe-qt)
y=0.00175-0.05824x
R2=0.9098
t (min)
(h)
t/qt
y=0.0502x+0.0126
R2=0.9999
t (min)

◂**Fig. 2** Effect of reaction time **a**, initial pH **b**, dosage **c** and co-existing ions **d** on the removal of U(VI) by nZVI/BC600. **g**, **h** Kinetic model parameters for the adsorption of U(VI)

Results and discussion

High-efficiency removal of U(VI) from aqueous solution

Experimental results on the removal of U(VI) with two types of adsorbents

We first compared the U(VI) removal rates of both Zn-BC600 and nZVI/Zn-BC600 under the same condition. The U(VI) removal rate and adsorption quantity of nZVI/BC600 had significantly higher (99.68%) than that of BC600 (90.5%), the removal rate of U(VI) reached 99.68% with nZVI/BC600 materials, while reached 90.50% with BC600.

We compared the effect of reaction time on the removal rate of U(VI) from the aqueous solution. As shown in Fig. 2a, U(VI) was rapidly removed within the first 25 min, even the removal capability of U(VI) reached 92.9% within 2 min, which was due to the large driving force and fast adsorption rate in the initial stage of the reaction. As the reaction continued, the driving force of adsorption and concentration gradient gradually decreased, concentration gradient gradually decreased resulting in slower adsorption rate through microporous channels [64], and the reaction capacity slowed down gradually. The removal rate of U(VI) in the solution reached equilibrium at 30 min, with the highest removal rate reaching 99.3%.

Solution pH was an important parameter affecting U(VI) removal, as it not only determined the U(VI) speciation but also the properties of the adsorbent. Batch experiments were carried out at different initial pH values to investigate the effect of pH on U(VI) removal capacity of nZVI/BC600. As shown in Fig. 2b, nZVI/BC600 offered a significant removal capacity for U(VI) with the pH ranging from 4.5 to 8.5, indicating that the weak acidic environment was more conducive to the removal of U(VI) by nZVI/BC600 [65, 66]. Because under acidic conditions, U(VI) in the solution mainly exists in the form of uranyl ion UO_2^{2+}, which was a dissociative state, and UO_2^{2+} was easy to be adsorbed and reduced to UO_2 by nZVI/BC600. However, under alkaline conditions, nZVI/BC600 pair U(VI) would react with OH^- in the solution to form iron hydroxide precipitation, which precipitated on the surface of nZVI/BC600, blocking the adsorption/reaction sites and hindering the electron transfer process, therefore, it was not conducive to the removal of U(VI).

Effects of varying nZVI/BC600 dosage (0.05 g/L to 1.0 g/L) were investigated on the removal rate of U(VI). Figure 2c showed that U(VI) removal rate increased from 82.27% to 99.68% with increasing amount of the dosage, and then reached a plateau. The removal rate of U(VI) increased significantly with increasing dosage up to 0.5 g/L, the quantity of the dissolved iron was 404.858 mg/L. Partially dissolving the iron nanoparticles may become a limitation in the prepared adsorbent. When the dosage was less than 0.5 g/L, the removal rate of U(VI) increased significantly by enhancing the dosage of nZVI/BC600, the maximum adsorption capacity was 19.94 mg/g, and the concentration of U(VI) in the solution was 0.032 mg/L, which met the emission standard. When the dosage increased, the active sites on the surface of nZVI/BC600 had reached the saturation state, thus, the removal rate of material to U(VI) basically had begun to flatten out.

As can be seen from Fig. 2d, the removal rate of U(VI) reduced as the starting U(VI) concentration increased, the adsorption amount of U(VI) increased, and the uranium concentration of the solution increased after the reaction. The clearance rate of U(VI) was greater than 99% in all cases when the initial U(VI) content was less than 10 mg/L. When the starting concentration of U(VI) was 100 mg/L, the removal rate was 75.13% and the adsorption amount was 150.27 mg/g. This was mostly due to a relative excess of nZVI/BC600 in the solution when the initial U(VI) concentration was low, as well as a larger surface area and a greater number of active sites for adsorption reaction, resulting in a higher U(VI) removal efficiency. The relative rose in U(VI) concentration in solution creates enough active sites on the adsorbent's surface to adsorb more uranyl ions, and therefore the adsorption quantity increases. When the initial U(VI) concentration was larger, the number of active sites for the adsorption reaction on nZVI/BC600 was reduced, resulting in a slower removal rate.

Here six common ions were chosen to investigate their effects on the removal efficiency of U(VI), since the actual uranium-bearing wastewater often contains other kinds of co-existing ions. As can be seen in Fig. 2e, certain inhibitory effects appeared on the removal of U(VI) by nZVI/BC600 in the presence of divalent cations (Mn^{2+}, Ca^{2+} and Mg^{2+}), which may be caused by their competitive sorption with uranyl ions towards nano zerovalent iron. The effect of three ions on the removal of U(VI) from nZVI/BC600 was $Ca^{2+} > Mg^{2+} > Mn^{2+}$. We observed that under this experimental condition, regarding the effects of anions (HCO_3^-, SO_4^{2-} and PO_4^{3-}), removal rate of U(VI) was not affected by both HCO_3^- and SO_4^{2-} in the solution, whereas it decreased remarkably in the presence of PO_4^{3-} as shown in Fig. 2f. In addition, negative ion PO_4^{3-} had a great influence on it, the adsorption efficiency of U(VI) decreased sharply. The reason for this phenomenon was that maybe PO_4^{3-} and UO_2^{2+} formed a competitive relationship in the solution, thus reducing the nZVI/BC600 active adsorption sites, beyond that, PO_4^{3-} may also be complexed with UO_2^{2+} to form complexes that were stable and difficult to react with nZVI,

and uranyl phosphate complexes such as $UO_2HPO_{4(aq)}$, $UO_2PO_4^-$, $UO_2H_2PO_4^+$ were formed by the complexation of PO_4^{3-} and UO_2^{2+}, greatly reduced the removal efficiency of U(VI).

In order to further study the kinetic behavior of adsorption of U(VI) on nZVI/BC600, the kinetic curves of adsorption of U(VI) on nZVI/BC600 were fitted and analyzed by pseudo-first-order and pseudo-second-order kinetic models, and the linear Eqs. (4) and (5).

$$\ln(q_e - q_t) = \ln q_e - k_1 t \tag{4}$$

$$\frac{t}{q_t} = \frac{1}{k_2 q_e^2} + \frac{t}{q_e} t \tag{5}$$

where q_t (mg/g) is the adsorption capacity at time t; q_e (mg/g) is the adsorption capacity when the adsorption reaches the dynamic equilibriuam; and k_1 (min^{-1}) and k_2 (g/(mg·min)) are the adsorption rate constants of the pseudo-first-order and pseudo-second-order models, respectively. Figure 2g, h showed that the pseudo-second-order model gave higher correlation coefficient ($R^2 = 0.9999$) than pseudo-first-order model ($R^2 = 0.9098$), and the q_e calculated from the model (19.881 mg/g) was very close to the experimental values (19.86 mg/g), which further indicated that the rate-limiting step in the adsorption process of U(VI) removal was chemical adsorption rather than physical diffusion. This result was consistent with that in the particle-grain model proposed by Vilardi et al. [67].

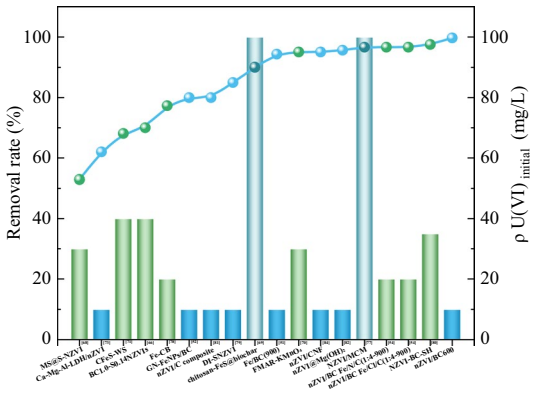

Fig. 3 Comparison of uranium removal efficiency between nZVI/BC600 and other different biochar-supported zero-valent iron materials

Comparison of U(VI) removal rates from previous literatures

Comparison of the uranium removal efficiency of zero-valent iron materials supported by different biochar in Fig. 3. It suggested that nZVI/BC600 was a promising environmental material for the remediation of U(VI). When $\rho(U(VI))_{initial} = 10$ mg/L, the adsorption equilibrium time of biochar carriers such as Fe-BC(900) [68] and GN-FeNPs/BC [69] for U(VI) was less than 97% removal efficiency after 40 min of reaction for lower uranium concentrations. When $\rho(U(VI))_{initial} = 10$~100 mg/L, the adsorption equilibrium time of synthetic biochar carriers such as Fe-CB [70] and nZVI/BC FeN/C(1:4-900) [71] for U(VI) was approximately 120 min after the reaction, and the removal efficiency was less than 98% for higher uranium concentrations. Furthermore, The iron-carbon ratios of GN-FeNPs/BC and nZVI/BC FeN/C(1:4-900) materials were 2:1 and 1:4, respectively, and this experiment synthesized the Fe:C ratio of nZVI/BC600 was 1:5. The U(VI) removal effectiveness of nZVI/BC600 was much greater (99.68%) within 0.5 h when compared to other synthetic biochar loaded with zero-valent iron nanoparticles. Thus, the nZVI/BC600 presented a superior potential for environmental application by compared with the adsorption capacity of other materials (Table 1).

Removal mechanism of U(VI) and comparison

Based on the above analysis results, the adsorption mechanism of U(VI) by nZVI/BC600 was proposed. Figure 4a was the magnetization curve of nZVI/BC600, indicating that nZVI/BC600 can be effectively separated from the solution at the end of uranyl absorption. Figure 4b was the XRD spectrum of nZVI/BC600, and the typical peaks were 31.72°, 34.36°, 36.24°, 47.48°, 56.52°, 62.84°, 67.84°, 69°, corresponding to the $ZnCl_2$ (PDF#79-0206), respectively.

Table 1 Comparison of U(VI) removal capacity of nZVI/BC600 with other zero-valent iron-containing biochar

Adsorbents	Q_{max} ($mg \cdot g^{-1}$)	Removal rate (%)	pH	T (K)	Time (h)	References
LDH@nZVI	176.0	90.00	5	298	1	[24]
Fe-PANI-GA	350.47	–	5.5	298	0.3	[25]
CMC-ZVI	20.00	87.00	6	294	2	[26]
CMC–INP	322.58	–	5	298	30	[27]
MWCNTs/ZIF-8	200.77	93.36	5	298	1	[29]
NZVI/CFA	147.6	48.33	6	298	1	[30]
nZVI@SA/CMC-Ca	180.0	93.00	4	298	1	[36]
nZVI/BC600	19.94	99.68	5.5	298	0.5	This study

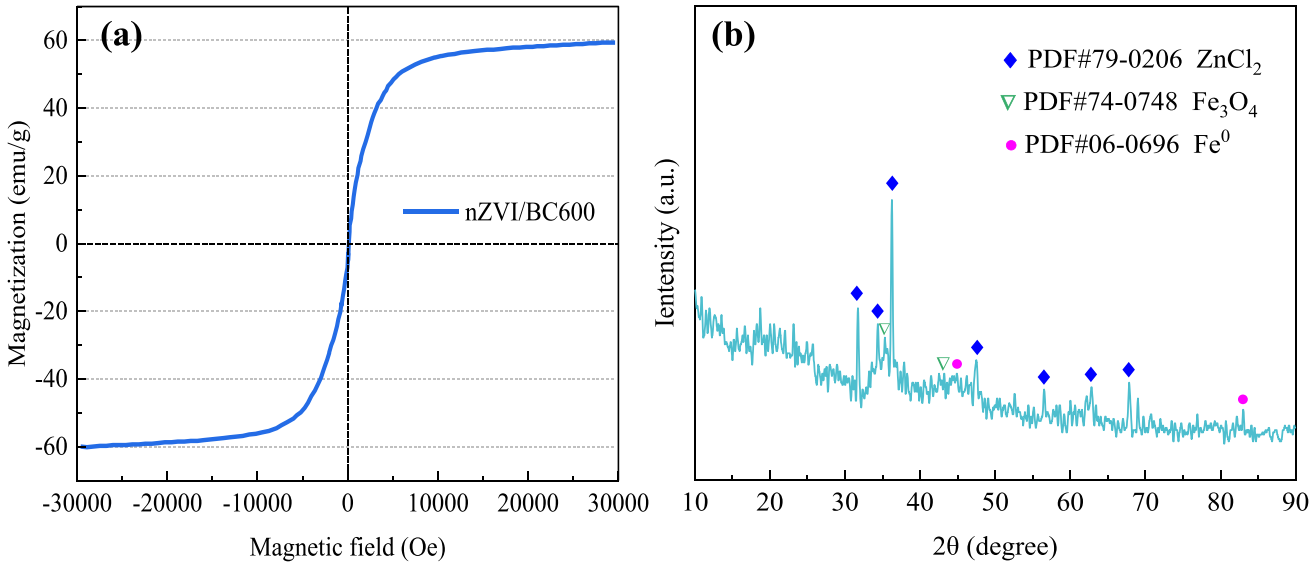

Fig. 4 Magnetization curve **a** and XRD spectrum **b** of nZVI/BC600

The typical peaks were 31.72° and 34.4° corresponding to the Fe_3O_4 (PDF#74-0748). The characteristic peaks of nZVI at 44.92° and 83° were observed from the figure, indicating that zero-valent iron exists in nZVI/BC600. It was indicated that the prepared adsorbent was modified with zero-valent iron nanoparticles.

To demonstrate the mechanism of U(VI) removal by nZVI/BC600, SEM and EDS characterization analysis were carried out for the materials before and after the reaction. The SEM images of BC600 were illustrated in Fig. 5a, b. The BC600 has a high porous structure and rough surface, which can provide adsorption sites for nZVI loading. It was observed that many substances of different sizes and shapes were distributed on the surface of activated carbon, which may be zinc particles formed on the surface of activated carbon during the modification process and it was consistent with the results of others' research [57]. Figure 5c, d showed the SEM images of nZVI/BC600 after loading. We observed that there were many spherically similar particles on the surface of the material, which had small particle sizes and were evenly distributed on the surface of activated carbon with good dispersion. It was inferred that the load of nZVI was distributed uniformly on the surface of BC600, suggesting that the carrier of nZVI, BC600 effectively hinders its aggregation and agglomeration [72]. Combined with EDS characterization diagram of nZVI/BC600 (Fig. 5g), the weight percentage of iron was 17.84%, and the appearance of iron further confirmed that nZVI has been successfully loaded on BC600. Figure 5e, f showed the SEM images of nZVI/BC600 after the reaction. Compared with the image of nZVI/BC600 before the reaction, new substances were generated on its surface with denser distribution after the reaction. In combination with EDS adsorption test, the element composition on the surface of nZVI/BC600 was shown in Fig. 5g, h. Obviously, there were apparent adsorption peaks of U can be observed as expected, indicating that U had been successfully adsorbed onto the surface of nZVI/BC. The weight ratio of iron (8.52%) was slightly lower than that before the reaction, indicating that iron participated in the reaction and was partially dissolved in the solution. Figure 5i showed the results of mapping of several elements (C, O, U and Fe) on the residual solid phase after the reaction. The appearance of U indicates that U or a substance of zero valence iron containing U was adsorbed on the surface of the material. Furthermore, it can be seen from Fig. 5i that the distribution of iron, uranium and oxygen elements on the surface of the residual solid after reaction were basically the same, indicating that some oxide was formed during the removal of U(VI) by nZVI/BC600 and uranium was adsorbed or reduced on the surface.

Figure 6 showed the FT-IR spectra of activated carbon BC600 before nZVI modification and nZVI/BC600 before and after U(VI) adsorption. It can be seen from the figure that the main characteristic peaked of the material surface before or after the reaction appear in 611~613 cm^{-1}, 1059 cm^{-1}, 2907~2912 cm^{-1} and 3389 cm^{-1}. A relatively broad peak at 3389 cm^{-1} of the sample before the adsorption test was attributed to stretching vibration of the -OH moiety [73]. The corresponding peak at 2907~2912 cm^{-1} was the C–H bond on saturated C, the stretching vibration peak of B-O bond in potassium borohydride at 1059 cm^{-1}, and the peak of wave number at 611–613 cm^{-1} corresponded to the peak of Fe–O stretching vibration of iron oxide, which further indicated that the nZVI was successfully loading on the

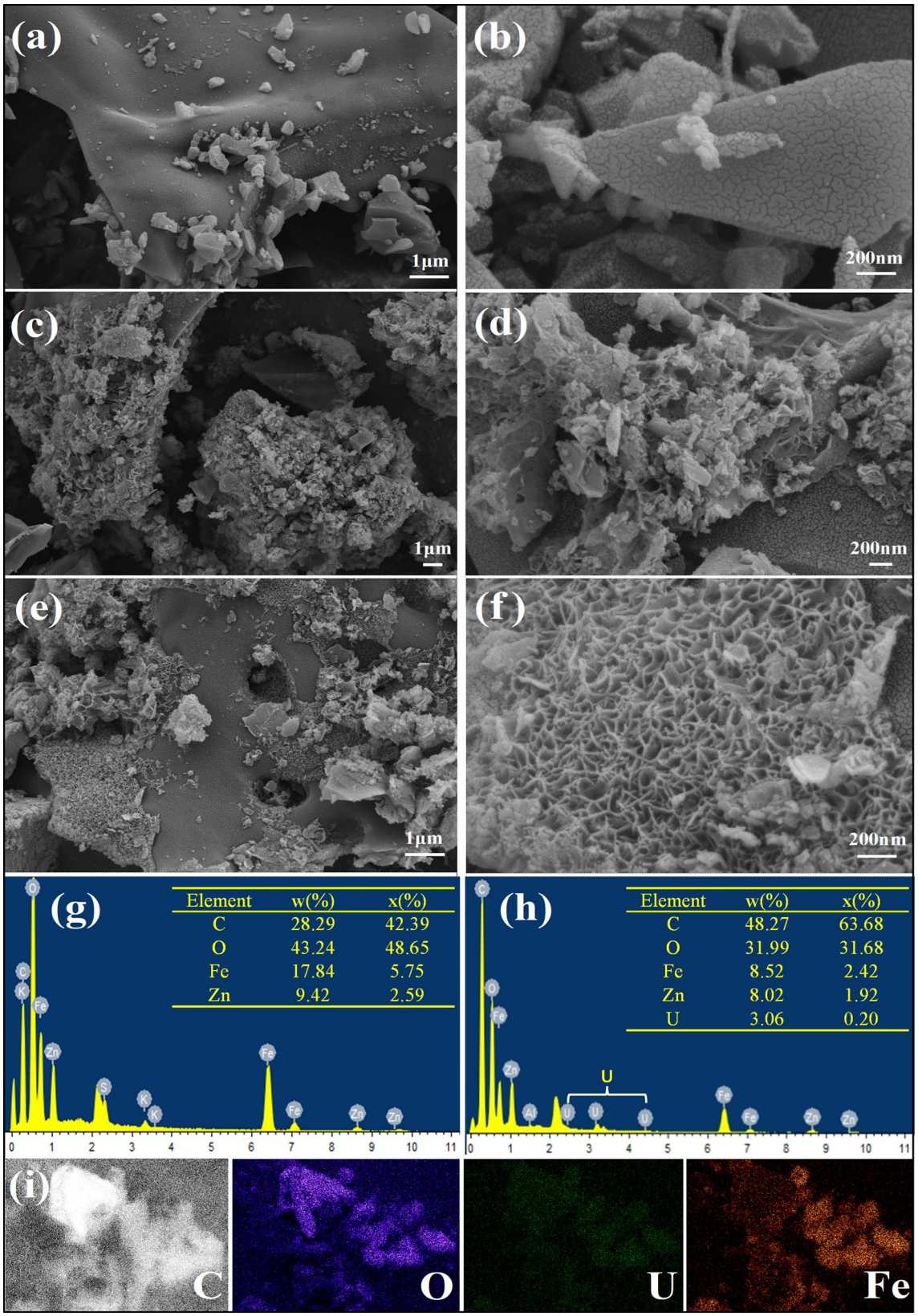

Fig. 5 SEM images of BC600 **a**, **b**, nZVI/BC600 before the reaction **c**, **d**, SEM images of nZVI/BC600 after the reaction **e**, **f**, EDS characterization diagram of nZVI/BC600 before **g** and after **h** the reaction, and Mapping spectra **i** of C, O, U, Fe after the reaction

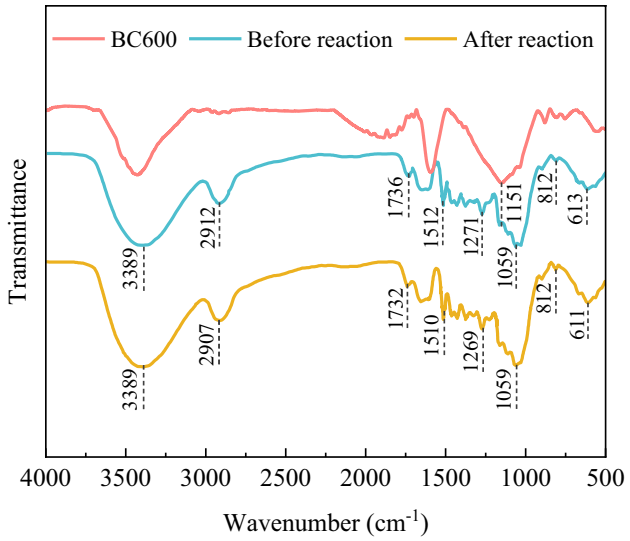

Fig. 6 FT-IR spectra of nZVI/BC600 before and after reaction with U(VI)

activated carbon. The wave number 1510~1512 cm^{-1} was the C=C stretching vibration peak [74], the wave numbers 1645~1649 cm^{-1} and 1732~1736 cm^{-1} were the C=O correspond to stretching vibration peaks, which retained the original functional groups of activated carbon. The absorption peaks corresponding to –OH, C–O and C=O groups shifted to the lower wave number after adsorption, which was speculated to be mainly due to the combination with U(VI) groups in the adsorption process and related to the redox of U(VI).

In order to prove that uranium participates in the reaction and explore the change of valence state after reaction, XPS was a very standard method to characterize the oxidation states of uranium [75]. Figure 7a showed XPS survey spectra of the samples before and after the reaction, the peaks of carbon, iron, and uranium observed from the overall spectrum further indicate that the nZVI/BC600 successfully immobilized uranium in the aqueous solution. As shown in Fig. 7b, the U 4f high-resolution spectra indicated that the main peaks U $4f_{7/2}$ (~382.1 eV) and U $4f_{5/2}$ (~392.3 eV) could both decompose into two peaks, which indicated there were two chemical states of U in the solids. The binding energy separation between the primary spin–orbit split peaks and their associated satellite peaks were 8.2 eV and 3.7 eV. Compared to the results of Ilton' research [76], the primary spin–orbit splitting peaks of U(VI) and U(V) had the corresponding satellites, and the binding energy distances between them were approximately 4.0 eV and 7.8~8.5 eV. The majority of investigations have discovered that during the Fe(II)-induced transition of ferrite to needle ferrite, the majority of the uranium in solution becomes lodged in the needle ferrite structure as U(V), indicating that U(V) was an effective retention pathway for U in iron oxides [77–80]. U(VI) was likewise reduced to U(V) by Fe(II) in the work of Xie' research [75].

In addition, as shown in Fig. 7c, d, compared to before the reaction, the single C1s peak of the sample after reaction could be decomposed into three peaks at about 284.78 eV, 285.82 eV and 288.53 eV, which correspond to C–C and C–H, C–O and O–C=O, respectively. Figure 7e, f showed high-resolution Fe 2p spectra of the samples before and after the reaction, the Fe $2p_{3/2}$ peaks of the sample at~711.09 eV was narrower and stronger than their Fe $2p_{1/2}$ peaks at~724.98 eV after the reaction. According to the study, for the crystal structure of iron oxyhydroxides, three quarters of the Fe(III) cations of the γ-compounds were octahedral and one quarter tetrahedral, while all Fe(III) cations of the α-compounds were octahedral [81]. As shown, the Fe $2p_{3/2}$ spectra were well fitted by two peaks corresponding to octahedral and tetrahedral Fe(III), which indicate that the Fe precipitates were likely to be γ-compounds. Figure 8 showed schematic diagram of the proposed mechanisms for the reduction and sorption of U(VI) by nZVI/BC600. Accordingly, nZVI/BC600 transforms U(VI) to U(IV) or U(V), confirming that the major modes of action were adsorption and reductive immobilization.

Conclusions

In this study, $ZnCl_2$ was used to modify peanut shells activated carbon, and then nZVI was loaded on it to achieve efficient removal of U(VI) from wastewater. Through characterization and a series of adsorption tests, the main conclusions were as follows:

1. The results of batch experiments showed that the dosage of nZVI/BC600 was positively correlated with the U(VI) removal efficiency to reach an adsorption equilibrium within 30 min. When the initial pH of the solution was 4.5~6, the dosage was 0.5 g/L, and the reaction time reached 30 min, the removal efficiency of U(VI) by nZVI supported by activated carbon was the best, with 99.68% removal rate. The U(VI) adsorption behavior of nZVI/BC600 conformed to the pseudo-secondary adsorption model, and mainly consisted of chemical adsorption ($R^2 = 0.9999$).
2. Compared with the removal efficiency of U(VI) by nZVI/BC600 and BC600. The removal efficiency of U(VI) by nZVI/BC600 was improved by 9.18%, with prominent advantage, which could meet the discharge standard for uranium-containing wastewater ($\rho(U(VI)) \leq 10$ mg/L).
3. SEM–EDS and Mapping analyses were utilized in this investigation to demonstrate that nZVI was uniformly distributed on the surface of BC600 activated carbon,

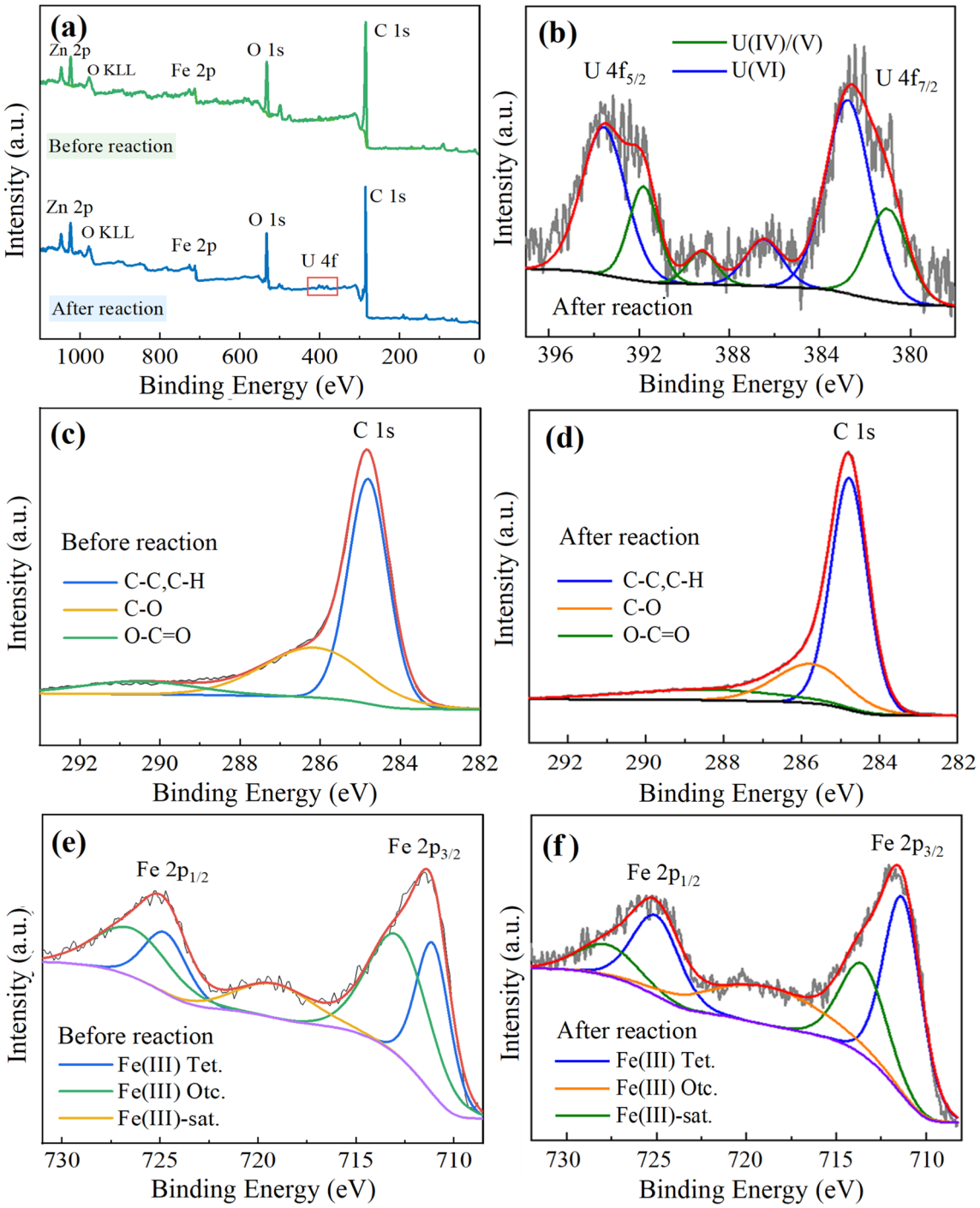

Fig. 7 XPS spectra of the samples before and after the reaction of nZVI/BC600 with U(VI)

which prevented agglomeration of zero-valent iron. Furthermore, U(VI) was successfully adsorbed on the nZVI/BC600 surface, resulting in surface complexes. FT-IR and XPS investigation suggested that functional groups such as -OH, C-O and C = O, zero-valent iron nanoparticles, iron oxyhydroxides, and iron oxides and hydroxides were found to perform adsorption and reduction roles in the removal of U(VI) by nZVI/BC600 in FT-IR and XPS investigations. Therefore, the removal of U(VI) by nZVI/BC600 was occurred through U(VI) adsorption and its subsequent reduction to U(IV) or U(V).

To sum up, the $ZnCl_2$ modified activated carbon loading nZVI composite material was economical and efficient,

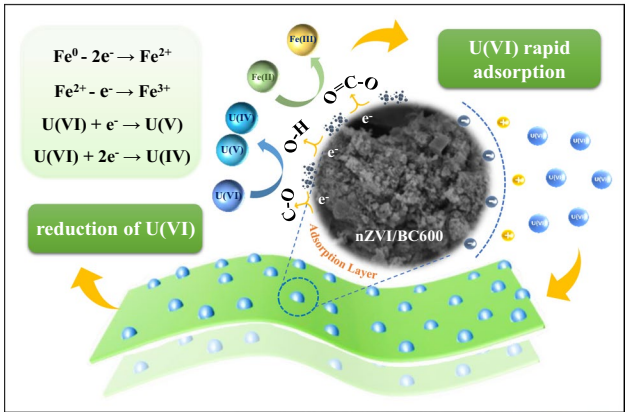

Fig. 8 Schematic diagram of the proposed mechanisms for the reduction and sorption of U(VI) by nZVI/BC600

easy to operate and pollution-free. The material not only had developed pore structure, high specific surface area and high surface activity characteristics of activated carbon, but also reduced agglomeration and significantly improved the reduction and adsorption performance of nZVI, due to the swelling and pore forming effect of $ZnCl_2$ modification. Beyond that, on account of the magnetic signature of nZVI, the material can be recovered and reused. Therefore, this composite material has great application potential in the treatment of low-concentration uranium-containing wastewater.

Acknowledgements This work was supported by the National Natural Science Foundation of China (11705082 and 51874180) and Natural Science Foundation of Hunan Province (2023JJ30513) as well as Research Project of Education Department of Hunan Province (22A0303).

Declaration

Competing interest The authors declare that they have no known competing financial interests or personal relationships that could have appeared to influence the work reported in this paper.

References

1. Sheng L, Fein JB (2014) Uranium reduction by *Shewanella oneidensis* MR-1 as a function of $NaHCO_3$ concentration: surface complexation control of reduction kinetics. Environ Sci Technol 48(7):3768–3775. https://doi.org/10.1021/es5003692
2. Tan WF, Li Y, Guo F, Wang YC, Ding L, Mumford K, Lv JW, Deng QW, Fang Q, Zhang XW (2020) Effect of *Leifsonia* sp. on ret ardation of uranium in natural soil and its potential mechanisms. J Environ Radioact 217:106202. https://doi.org/10.1016/j.jenvrad.2020.106202
3. Pan Z, Bártová B, LaGrange T, Butorin SM, Hyatt NC, Stennett MC, Kvashnina KO, Bernier-Latmani R (2020) Nanoscale mechanism of UO_2 formation through uranium reduction by magnetite. Nat Commun 11(1):4001. https://doi.org/10.1038/s41467-020-17795-0
4. Hu C, Liu C, Huang G, Li T, Xu H, Hu X, Xu C (2020) Analysis of total Uranium concentration in drinking water source. Chin J Radiol Health 29:628–631. https://doi.org/10.13491/j.issn.1004-714X.2020.06.013
5. Li XY, Zhang M, Liu YB, Li X, Yang B, Hua R, Liu Y (2015) Effect of ionic strength, anion, cation and humic acid on removal of U(VI) in aqueous solution by nanoscale zero-valent iron. Chin J Nonferrous Metals 25:3505–3512. https://doi.org/10.19476/j.ysxb.1004.0609.2015.12.029
6. He S, Yang Z, Cui X, Zhang X, Niu X (2020) Fabrication of the novel Ag-doped SnS_2@$InVO_4$ composite with high adsorption-photocatalysis for the removal of uranium (VI). Chemosphere 260:127548. https://doi.org/10.1016/j.chemosphere.2020.127548
7. Yan S, Chen Y, Xiang W, Bao Z, Liu C, Deng B (2014) Uranium(VI) reduction by nanoscale zero-valent iron in anoxic batch systems: the role of Fe(II) and Fe(III). Chemosphere 117:625–630. https://doi.org/10.1016/j.chemosphere.2014.09.087
8. Li X, Zhang M, Liu Y, Li X, Liu Y, Hua R, He C (2013) Removal of U(VI) in aqueous solution by nanoscale zero-valent iron(nZVI). Expo Health 5:31–40. https://doi.org/10.1007/s12403-013-0084-4
9. Crane RA, Dickinson M, Popescu IC, Scott TB (2011) Magnetite and zero-valent iron nanoparticles for the remediation of uranium contaminated environmental water. Water Res 45(9):2931–2942. https://doi.org/10.1016/j.watres.2011.03.012
10. Jing C, Landsberger S, Li YL (2017) The application of illite supported nanoscale zero valent iron for the treatment of uranium contaminated groundwater. J Environ Radioact 175:1–6. https://doi.org/10.1016/j.jenvrad.2017.04.003
11. Jing C, Li YL, Landsberger S (2016) Review of soluble uranium removal by nanoscale zero valent iron. J Environ Radioact 164:65–72. https://doi.org/10.1016/j.jenvrad.2016.06.027
12. Mueller NC, Braun J, Bruns J, Černík M, Rissing P, Rickerby D, Nowack B (2011) Application of nanoscale zero valent iron (NZVI) for groundwater remediation in Europe. Environ Sci Pollut Res 19:550–558. https://doi.org/10.1007/s11356-011-0576-3
13. Singh R, Misra V, Singh RP (2011) Removal of Cr(VI) by nanoscale zero-valent iron (nZVI) from soil contaminated with tannery wastes. Bull Environ Contam Toxicol 88:210–214. https://doi.org/10.1007/s00128-011-0425-6
14. Zhou Z-Y, Tian N, Li J-T, Broadwell I, Sun S-G (2011) Nanomaterials of high surface energy with exceptional properties in catalysis and energy storage. Chem Soc Rev 88:210–214. https://doi.org/10.1039/c0cs00176g
15. Hu Z, Wang H, Liu R, Hu B, Qiu M (2022) Removal of U(vi) from aqueous solutions by an effective bio-adsorbent from walnut shell and cellulose composite-stabilized iron sulfide nanoparticles. RSC Adv 12(5):2675–2683. https://doi.org/10.1039/d1ra08087c
16. Sun Y, Ding C, Cheng W, Wang X (2014) Simultaneous adsorption and reduction of U(VI) on reduced graphene oxide-supported nanoscale zerovalent iron. J Hazard Mater 280:399–408. https://doi.org/10.1016/j.jhazmat.2014.08.023
17. De León MA, Sergio M, Bussi J, Ortiz de la Plata GB, Cassano AE, Alfano OM (2014) Application of a montmorillonite clay modified with iron in photo-Fenton process. Comparison with goethite and nZVI. Environ Sci Pollut Res 22:864–869. https://doi.org/10.1007/s11356-014-2681-6
18. Jiang Z, Lv L, Zhang W, Du Q, Pan B, Yang L, Zhang Q (2011) Nitrate reduction using nanosized zero-valent iron supported by polystyrene resins: role of surface functional groups. Water Res 45(6):2191–2198. https://doi.org/10.1016/j.watres.2011.01.005
19. Kakavandi B, Kalantary RR, Farzadkia M, Mahvi AH, Esrafili A, Azari A, Yari AR, Javid AB (2014) Enhanced chromium (VI) removal using activated carbon modified by zero valent iron and silver bimetallic nanoparticles. J Environ Health Sci Eng 12:1–10. https://doi.org/10.1186/s40201-014-0115-5

20. Li ZJ, Wang L, Yuan LY, Xiao CL, Mei L, Zheng LR, Zhang J, Yang JH, Zhao YL, Zhu ZT, Chai ZF, Shi WQ (2015) Efficient removal of uranium from aqueous solution by zero-valent iron nanoparticle and its graphene composite. J Hazard Mater 290:26–33. https://doi.org/10.1016/j.jhazmat.2015.02.028
21. Saleh TA, Naeemullah N, Tuzen M, Sarı A (2016) Polyethylenimine modified activated carbon as novel magnetic adsorbent for the removal of uranium from aqueous solution. Chem Eng Res Des 117:218–227. https://doi.org/10.1016/j.cherd.2016.10.030
22. Sheng G, Yang P, Tang Y, Hu Q, Li H, Ren X, Hu B, Wang X, Huang Y (2016) New insights into the primary roles of diatomite in the enhanced sequestration of UO_2^{2+} by zerovalent iron nanoparticles: An advanced approach utilizing XPS and EXAFS. Appl Catal B 193:189–197. https://doi.org/10.1016/j.apcatb.2016.04.035
23. Tseng H-H, Su J-G, Liang C (2011) Synthesis of granular activated carbon/zero valent iron composites for simultaneous adsorption/dechlorination of trichloroethylene. J Hazard Mater 192(2):500–506. https://doi.org/10.1016/j.jhazmat.2011.05.047
24. Yu S, Wang X, Liu Y, Chen Z, Wu Y, Liu Y, Pang H, Song G, Chen J, Wang X (2019) Efficient removal of uranium(VI) by layered double hydroxides supported nanoscale zero-valent iron: a combined experimental and spectroscopic studies. Chem Eng J 365:51–59. https://doi.org/10.1016/j.cej.2019.02.024
25. Chen L, Feng S, Zhao D, Chen S, Li F, Chen C (2017) Efficient sorption and reduction of U(VI) on zero-valent iron-polyaniline-graphene aerogel ternary composite. J Colloid Interface Sci 490:197–206. https://doi.org/10.1016/j.jcis.2016.11.050
26. Zhao X, Liu W, Cai Z, Fu J, Duan J, Zhao D, Bozack M, Feng Y (2020) Reductive immobilization of uranium by stabilized zero-valent iron nanoparticles: effects of stabilizers, water chemistry and long-term stability. Colloids Surf A Physicochem Eng Aspects 604:125315. https://doi.org/10.1016/j.colsurfa.2020.125315
27. Filip P, Popescu I-C, Humelnicu D, Humelnicu I, Scott TB, Crane RA (2013) Removal of uranium (VI) from aqueous systems by nanoscale zero-valent iron particles suspended in carboxy-methyl cellulose. J Nucl Mater 443(1–3):250–255. https://doi.org/10.1016/j.jnucmat.2013.07.018
28. Pang H, Wu Y, Huang S, Ding C, Li S, Wang X, Yu S, Chen Z, Song G, Wang X (2018) Macroscopic and microscopic investigation of uranium elimination by Ca–Mg–Al-layered double hydroxide supported nanoscale zero valent iron. Inorg Chem Front 5(10):2657–2665. https://doi.org/10.1039/c8qi00779a
29. Zheng H, Ren X, Zhang X, Song G, Chen D, Chen C (2020) Mutual effect of U(VI) and phosphate on the reactivity of nanoscale zero-valent iron (nZVI) for their co-removal. J Mol Liquids 297:111853. https://doi.org/10.1016/j.molliq.2019.111853
30. Chen Z, Xing J, Pu Z, Wang X, Yang S, Wei B, Ai Y, Li X, Chen D, Wang X (2018) Preparation of nano-Fe^0 modified coal fly-ash composite and its application for U(VI) sequestration. J Mol Liq 266:824–833. https://doi.org/10.1016/j.molliq.2018.05.118
31. Hu B, Mei X, Li X, Hu J, Xu D, Ma J, Huang Y (2017) Decontamination of U(VI) from nZVI/CNF composites investigated by batch, spectroscopic and modeling techniques. J Mol Liq 237:1–9. https://doi.org/10.1016/j.molliq.2017.04.084
32. Hao T, Shu Z, Hongwei P, Jiaqi W, Xiangxue W, Gang S, Shujun Y (2021) Insights into enhanced removal of U(VI) by melamine sponge supported sulfurized nanoscale zero-valent iron. J Clean Prod 329:129662. https://doi.org/10.1016/j.jclepro.2021.129662
33. Pang H, Diao Z, Wang X, Ma Y, Yu S, Zhu H, Chen Z, Hu B, Chen J, Wang X (2019) Adsorptive and reductive removal of U(VI) by dictyophora indusiate-derived biochar supported sulfide NZVI from wastewater. Chem Eng J 366:368–377. https://doi.org/10.1016/j.cej.2019.02.098
34. Zhu H, Jia Y, Wu X, Wang H (2009) Removal of arsenic from water by supported nano zero-valent iron on activated carbon. J Hazard Mater 172(2–3):1591–1596. https://doi.org/10.1016/j.jhazmat.2009.08.031
35. Pang H, Zhang E, Zhang D, Wang X, Zhao B, Liu L, Ma X, Song G, Yu S (2022) Precursor impact and mechanism analysis of uranium elimination by biochar supported sulfurized nanoscale zero-valent iron. J Environ Chem Eng 10(2):107288. https://doi.org/10.1016/j.jece.2022.107288
36. Hu S, Lin X, Zhao W, Luo X (2017) Efficient simultaneous removal of U(VI) and Cu(II) from aqueous solution using core–shell nZVI@SA/CMC-Ca beads. J Radioanal Nucl Chem 315:223–235. https://doi.org/10.1007/s10967-017-5662-7
37. Wang JQ, Duan HW, Tang H, Yu SJ, Zhu HT, Wang XX (2020) Carbothermic synthesis of carbon-supported zero-valent iron material for removal of U(VI) from aqueous solution. J Inorgan Mater 35:373–380. https://doi.org/10.15541/jim20190378
38. Liu C, Lu J, Tan Y, Chen B, Yang P (2022) Removal of U(VI) from wastewater by sulfhydryl-functionalized biomass carbon supported nano-zero-valent iron through synergistic effect of adsorption and reduction. Mater Sci Eng B 284:115891. https://doi.org/10.1016/j.mseb.2022.115891
39. Liu H, Li M, Chen T, Chen C, Alharbi NS, Hayat T, Chen D, Zhang Q, Sun Y (2017) New synthesis of nZVI/C composites as an efficient adsorbent for the uptake of U(VI) from aqueous solutions. Environ Sci Technol 51(16):9227–9234. https://doi.org/10.1021/acs.est.7b02431
40. Wang W, Zhou M, Mao Q, Yue J, Wang X (2010) Novel NaY zeolite-supported nanoscale zero-valent iron as an efficient heterogeneous Fenton catalyst. Catal Commun 11(11):937–941. https://doi.org/10.1016/j.catcom.2010.04.004
41. Li Q, Wang H, Chen Z, He X, Liu Y, Qiu M, Wang X (2021) Adsorption-reduction strategy of U(VI) on NZVI-supported zeolite composites via batch, visual and XPS techniques. J Mol Liq 339:116719. https://doi.org/10.1016/j.molliq.2021.116719
42. Cruz MLD, Araño K, Pena EMD, Diaz LJL (2013) Nanoclay-supported zero-valent iron as an efficient adsorbent material for arsenic. Adv Mater Res 2322:296–304. https://doi.org/10.4028/www.scientific.net/AMR.686.296
43. Li C, Chen N, Zhao Y, Li R, Feng C (2016) Polypyrrole-grafted peanut shell biological carbon as a potential sorbent for fluoride removal: Sorption capability and mechanism. Chemosphere 163:81–89. https://doi.org/10.1016/j.chemosphere.2016.08.016
44. Lu L, Lin Y, Chai Q, He S, Yang C (2018) Removal of acenaphthene by biochar and raw biomass with coexisting heavy metal and phenanthrene. Colloids Surf A 558:103–109. https://doi.org/10.1016/j.colsurfa.2018.08.057
45. Xue DQ (2014) Magnetic properties of nano zerovalent iron particles coated with biopolymers. Trans Tech Publ Ltd 912:32–35. https://doi.org/10.4028/www.scientific.net/AMR.912-914.32
46. Crane RA, Scott T (2014) The removal of uranium onto carbon-supported nanoscale zero-valent iron particles. J Nanopart Res 16:1–13. https://doi.org/10.1007/s11051-014-2813-4
47. Lehmann J, Gaunt J, Rondon M (2006) Bio-char sequestration in terrestrial ecosystems—a review. Mitig Adapt Strat Glob Change 11:403–427. https://doi.org/10.1007/s11027-005-9006-5
48. He R, Yuan X, Huang Z, Wang H, Jiang L, Huang J, Tan M, Li H (2019) Activated biochar with iron-loading and its application in removing Cr (VI) from aqueous solution. Colloids Surf A Physicochem Eng Asp 579:123642. https://doi.org/10.1016/j.colsurfa.2019.123642
49. Wang C, Wang H, Cao Y (2018) Pb(II) sorption by biochar derived from Cinnamomum camphora and its improvement with ultrasound-assisted alkali activation. Colloids Surf A 556:177–184. https://doi.org/10.1016/j.colsurfa.2018.08.036

50. Yang F, Zhang S, Sun Y, Cheng K, Li J, Tsang DCW (2018) Fabrication and characterization of hydrophilic corn stalk biochar-supported nanoscale zero-valent iron composites for efficient metal removal. Biores Technol 265:490–497. https://doi.org/10.1016/j.biortech.2018.06.029
51. Zhou N, Wang Y, Huang L, Yu J, Chen H, Tang J, Xu F, Lu X, Zhong M-e, Zhou Z (2019) In situ modification provided by a novel wet pyrolysis system to enhance surface properties of biochar for lead immobilization. Colloids Surf A 570:39–47. https://doi.org/10.1016/j.colsurfa.2019.03.012
52. Su H, Fang Z, Tsang PE, Zheng L, Cheng W, Fang J, Zhao D (2016) Remediation of hexavalent chromium contaminated soil by biochar-supported zero-valent iron nanoparticles. J Hazard Mater 318:533–540. https://doi.org/10.1016/j.jhazmat.2016.07.039
53. Li H, Chen YQ, Chen S, Wang XL, Guo S, Qiu YF, Liu YD, Duan XL, Yu YJ (2017) Wheat straw biochar-supported nanoscale zerovalent iron for removal of trichloroethylene from groundwater. PLoS ONE 12(3):e0172337. https://doi.org/10.1371/journal.pone.0172337
54. Fan C, Chen N, Qin J, Yang Y, Feng C, Li M, Gao Y (2020) Biochar stabilized nano zero-valent iron and its removal performance and mechanism of pentavalent vanadium(V(V)). Colloids Surf A Physicochem Eng Asp 599:124882. https://doi.org/10.1016/j.colsurfa.2020.124882
55. Zhang S, Lyu H, Tang J, Song B, Zhen M, Liu X (2018) A novel biochar supported CMC stabilized nano zero-valent iron composite for hexavalent chromium removal from water. Chemosphere 217:686–694. https://doi.org/10.1016/j.chemosphere.2018.11.040
56. Yan J, Han L, Gao W, Xue S, Chen M (2014) Biochar supported nanoscale zerovalent iron composite used as persulfate activator for removing trichloroethylene. Biores Technol 175:269–274. https://doi.org/10.1016/j.biortech.2014.10.103
57. Li C, Zhang L, Gao Y, Li A (2018) Facile synthesis of nano ZnO/ZnS modified biochar by directly pyrolyzing of zinc contaminated corn stover for Pb(II), Cu(II) and Cr(VI) removals. Waste Manage 79:625–637. https://doi.org/10.1016/j.wasman.2018.08.035
58. Tang J, Lv H, Gong Y, Huang Y (2015) Preparation and characterization of a novel graphene/biochar composite for aqueous phenanthrene and mercury removal. Biores Technol 196:355–363. https://doi.org/10.1016/j.biortech.2015.07.047
59. Xia D, Tan F, Zhang C, Jiang X, Chen Z, Li H, Zheng Y, Li Q, Wang Y (2016) $ZnCl_2$ -activated biochar from biogas residue facilitates aqueous As(III) removal. Appl Surf Sci 377:361–369. https://doi.org/10.1016/j.apsusc.2016.03.109
60. Yu Y, An Q, Jin L, Luo N, Li Z, Jiang J (2019) Unraveling sorption of Cr (VI) from aqueous solution by $FeCl_3$ and ZnCl2-modified corn stalks biochar: implicit mechanism and application. Bioresour Technol 297:122466. https://doi.org/10.1016/j.biortech.2019.122466
61. Wang J, Chen N, Li M, Feng C (2017) Efficient removal of fluoride using polypyrrole-modified biochar derived from slow pyrolysis of pomelo peel: sorption capacity and mechanism. J Polym Environ 26:1559–1572. https://doi.org/10.1007/s10924-017-1061-y
62. Quan G, Sun W, Yan J, Lan Y (2014) Nanoscale zero-valent iron supported on biochar: characterization and reactivity for degradation of acid orange 7 from aqueous solution. Water Air Soil Pollut 225:1–10. https://doi.org/10.1007/s11270-014-2195-3
63. Wu Y, Pang H, Yao W, Wang X, Yu S, Yu Z, Wang X (2018) Synthesis of rod-like metal-organic framework (MOF-5) nanomaterial for efficient removal of U(VI): batch experiments and spectroscopy study. Sci Bull 63(13):831–839. https://doi.org/10.1016/j.scib.2018.05.021
64. Yu J, Jiang C, Guan Q, Ning P, Gu J, Chen Q, Zhang J, Miao R (2017) Enhanced removal of Cr(VI) from aqueous solution by supported ZnO nanoparticles on biochar derived from waste water hyacinth. Chemosphere 195:632–640. https://doi.org/10.1016/j.chemosphere.2017.12.128
65. Korichi S, Bensmaili A (2009) Sorption of uranium (VI) on homoionic sodium smectite experimental study and surface complexation modeling. J Hazard Mater 169(1–3):780–793. https://doi.org/10.1016/j.jhazmat.2009.04.014
66. Zhang C, Zhang W, Zhou XH (2009) Immobilization of U(VI) in solution by zero-valent iron. Uranium Min Metall 28(3):155–157. https://doi.org/10.3969/j.issn.1000-8063.2009.03.010
67. Vilardi G, Palma LD, Verdone N (2019) A physical-based interpretation of mechanism and kinetics of Cr(VI) reduction in aqueous solution by zero-valent iron nanoparticles. Chemosphere 220:590–599. https://doi.org/10.1016/j.chemosphere.2018.12.175
68. Ruan Y, Zhang H, Yu Z, Diao Z, Song G, Su M, La H, Chen D, Wang S, Kong L (2021) Phosphate enhanced uranium stable immobilization on biochar supported nano zero valent iron. J Hazard Mater 424:127119. https://doi.org/10.1016/j.jhazmat.2021.127119
69. Liu Q, Yiwen Xu, Guodong Z, Yilong H, Weifan L (2022) Removal of U(VI) from water by biochar supported green iron nanoparticles. Acta Materiae Compos Sinica 39(12):5934–5945. https://doi.org/10.13801/j.cnki.fhclxb.20211129.004
70. Wang J, Duan H, Tang H, Yu S, Zhu H, Wang X (2020) Carbothermic synthesis of carbon-supported zero-valent iron material for removal of U(VI) from aqueous solution. J Inorg Mater 35:373–380. https://doi.org/10.15541/JIM20190378
71. Zhang H, Ruan Y, Liang A, Shih K, Diao Z, Su M, La H, Chen D, Lu H, Kong L (2019) Carbothermal reduction for preparing nZVI/BC to extract uranium: Insight into the iron species dependent uranium adsorption behavior. J Clean Prod 239:117873. https://doi.org/10.1016/j.jclepro.2019.117873
72. Qian L, Liu S, Zhang W, Chen Y, Ouyang D, Han L, Yan J, Chen M (2018) Enhanced reduction and adsorption of hexavalent chromium by palladium and silicon rich biochar supported nanoscale zero-valent iron. J Colloid Interface Sci 533:428–436. https://doi.org/10.1016/j.jcis.2018.08.075
73. Zhai S, Li M, Wang D, Zhang L, Yang Y, Fu S (2019) In situ loading metal oxide particles on bio-chars: reusable materials for efficient removal of methylene blue from wastewater. J Clean Prod 220:460–474. https://doi.org/10.1016/j.jclepro.2019.02.152
74. Son E-B, Poo K-M, Chang J-S, Chae K-J (2017) Heavy metal removal from aqueous solutions using engineered magnetic biochars derived from waste marine macro-algal biomass. Sci Total Environ 615:161–168. https://doi.org/10.1016/j.scitotenv.2017.09.171
75. Xie Y, Fang Q, Li M, Wang S, Luo Y, Wu X, Lv J, Tan W, Wang H, Tan K (2019) Low concentration of Fe(II) to enhance the precipitation of U(VI) under neutral oxygen-rich conditions. Sci Total Environ 711:134827. https://doi.org/10.1016/j.scitotenv.2019.134827
76. Ilton ES, Bagus PS (2011) XPS determination of uranium oxidation states. Surf Interface Anal 43(13):1549–1560. https://doi.org/10.1002/sia.3836
77. Nico PS, Stewart BD, Fendorf S (2009) Incorporation of oxidized uranium into Fe (hydr)oxides during Fe(II) catalyzed remineralization. Environ Sci Technol 43(19):7391–7396. https://doi.org/10.1021/es900515q
78. Boland DD, Collins RN, Glover CJ, Payne TE, Waite TD (2014) Reduction of U(VI) by Fe(II) during the Fe(II)-accelerated transformation of ferrihydrite. Environ Sci Technol 48(16):9086–9093. https://doi.org/10.1021/es501750z
79. Boland DD, Collins RN, Payne TE, Waite TD (2011) Effect of amorphous Fe(III) oxide transformation on the Fe(II)-mediated reduction of U(VI). Environ Sci Technol 45(4):1327–1333. https://doi.org/10.1021/es101848a

80. Massey MS, Lezama-Pacheco JS, Jones ME, Ilton ES, Cerrato JM, Bargar JR, Fendorf S (2014) Competing retention pathways of uranium upon reaction with Fe(II). Geochim Cosmochim Acta 142:166–185. https://doi.org/10.1016/j.gca.2014.07.016
81. Mei H, Tan X, Tan L, Meng Y, Chen C, Fang M, Wang X (2018) Retention of U(VI) by the formation of Fe precipitates from oxidation of Fe(II). ACS Earth Space Chem 2(10):968–976. https://doi.org/10.1021/acsearthspacechem.8b00055